

Article

Simulation and Seasonal Characteristics of the Intra-Annual Heat Exchange Process in a Shallow Ice-Covered Lake

Fang Yang ¹, Weiyong Feng ^{2,3,*}, Leppäranta Matti ⁴, Yu Yang ⁵, Ioanna Merkouriadi ⁶, Rui Cen ⁷, Yangwei Bai ¹, Changyou Li ⁸ and Haiqing Liao ^{1,*}

¹ State Key Laboratory of Environmental Criteria and Risk Assessment, Chinese Research Academy of Environmental Sciences, Beijing 100012, China; yang.fang@craes.org.cn (F.Y.); baiyw@craes.org.cn (Y.B.)

² School of Spasce and Environment, Beihang University, Beijing 100191, China

³ Beijing Advanced Innovation Center for Big Data-Based Precision Medicine, Beihang University, Beijing 100191, China

⁴ Institute for Atmospheric and Earth System Research, University of Helsinki, 00014 Helsinki, Finland; matti.lepparanta@helsinki.fi

⁵ General Studies Teaching Department, Shengyang Institute of Engineering, Shengyang 110136, China; yangyu@sie.edu.cn

⁶ Earth Observation Programme, Finnish Meteorological Institute, 00560 Helsinki, Finland; ioanna.merkouriadi@fmi.fi

⁷ Department of Irrigation and Drainage, China Institute of Water Resources and Hydropower Research, Beijing 100089, China; qinr8168@sina.com

⁸ Water Conservancy and Civil Engineering College, Inner Mongolia Agricultural University, Hohhot 010018, China; nndlichangyou@163.com

* Correspondence: fengweiyong@buaa.edu.cn (W.F.); liaohq@craes.org.cn (H.L.)

Received: 16 July 2020; Accepted: 15 September 2020; Published: 22 September 2020



Abstract: The intra-annual heat exchange process has a considerable influence on the energy circulation, material metabolism, and ecological succession of lakes. The input and output of heat in an ice-covered lake provide the basic dynamic force driving changes in the biochemical state of the lake. Based on the heat balance between the lake surface and the atmosphere, we established a thermodynamic model for calculating the thermodynamic factors of shallow inland lakes during the ice and open seasons. The data of the Ulansuhai Lake, Inner Mongolia, from two years (2012 and 2013) are used to analyze the seasonal characteristics and associated influences of the heat budget on the ecosystem. The results indicated that the monthly mean lake temperature over the past 10 years was 1.7–2.2 °C lower than in the previous 50 years. The absorbed solar radiation reached up to 210 W/m² in 2012 and 179 W/m² in 2013, and there were clear differences in the heat budget between the ice-covered and open seasons. The mean net heat fluxes in the ice season were −33.8 and −38.5 W/m² in 2012 and 2013, respectively; while in the open season water, these fluxes were 62.5 and 19.1 W/m². In the simulations, the wind was an important factor for intensive evaporation in summer and the main driver of the ice cover formation patterns in winter, involving the transmission and diffusion of material and energy in the lake. The results provide a theoretical foundation for simulating ice cover growth and ablation processes in shallow lakes. They also present data on the ecological evolution in these lacustrine environments.

Keywords: ice season; energy budget; thermodynamic model; heat flux; Ulansuhai Lake

1. Introduction

Heat exchange between lakes and the atmosphere is an important part of lake water–atmosphere interaction, and the heat content of lakes provides a sensitive indicator of climate change [1,2]. The surface radiation budget and energy balance are the basis for research on land–atmosphere energy exchange. In recent years, studies have mainly focused on terrestrial ecosystems [3–5], and lake ecosystems have been investigated more frequently [6–11]. Compared with land areas, lake waters have a higher specific heat capacity and lower albedo, leading to substantial differences between lake–atmosphere and land–atmosphere energy exchange [12]. Therefore, investigating the lake surface radiation budget and energy balance is critical for understanding the lake–atmosphere heat exchange mechanisms and for elucidating the global energy budget [13]. Such work will also provide scientific background information for the management of lake ecosystems.

Because of the high specific heat capacity of lake waters, lake–atmosphere energy exchange is characterized by lower hysteresis and strength reduction, compared with land–atmosphere energy exchange. Thus, the land vs. water surface effect can produce a local temperature at the periphery the lake, influencing the local climate [14,15] and also the circulation of pollutants within the basin [16–18]. In cold regions especially, the heat budget in lakes has a direct effect on ice cover formation, which in turn has an impact on the lake ecosystem and resident organisms [1,19]. Thermodynamic processes in lakes are mainly controlled by meteorological conditions, while variation in the heat content of lakes is an important condition for aquatic habitats. To predict the impact of climate change on the lake water environment, numerous coupled climate models have been developed [20], such as Common Land Model [21] and Community Earth System Model 1 [22,23]. However, these models have been designed for deep lakes (~50 m) and do not apply to shallow lakes. Moreover, existing studies on the thermodynamic equilibrium in lakes are commonly conducted during the open season, and the lake water temperature is calculated mainly through climate models from the meteorological perspective [23]. For example, Cheng et al. [24] investigated the spatiotemporal distribution of radiation and energy budgets in the shallow Taihu Lake (2 m water depth) by fitting multiple evaporation models to this lake. They also simulated lake–atmosphere heat exchange by building a closed thermodynamic model in East Taihu Lake [24]. Using the CLM4, Deng et al. [25] modeled the heat and water fluxes in shallow lakes, including the Taihu Lake. Through analyzing the eddy diffusion parameters, Dai et al. [26] also simulated water temperature and variations of heat fluxes in Taihu Lake using a one-dimensional thermal diffusion model. They observed completely different heat variation patterns and water–atmosphere exchange characteristics in Taihu Lake to those in deep lakes [27]. Therefore, studies on the heat energy budget can provide information on phenomenological change for research on seasonally ice-covered shallow lakes [28–30].

Dimictic, cold climate lakes, such as Ulansuhai Lake in Inner Mongolia, are covered by ice and remain in a relatively stable state for several months in a year [31]. Generally, these lakes do not pose a threat to residents in the surrounding areas. Therefore such lakes have received little attention concerning their thermodynamic and hydrological processes. However, the ice cover plays an important role in water temperature, flow, and mixing in winter, and it also influences the lake–atmosphere heat exchange, resulting in a remarkable seasonal difference compared with the open-water season. This variation can lead to new problems in eutrophic lakes, where environmental self-remediation is delayed and even pollutants are aggregated. A deeper understanding of the intra-annual thermodynamic process in seasonally ice-covered lakes is required.

The present study is based on the thermodynamics in a shallow bay associated with freezing [32]. The objective was to establish a numerical model of a heat budget in a shallow lake in a cold and arid region, based on the lake–atmosphere exchange of matter and energy. The results provide a theoretical foundation for further research on ice-covered shallow lakes and ice thickness prediction models.

2. Materials and Methods

2.1. Study Area

Ulansuhai Lake ($40^{\circ}36'–41^{\circ}03' N$, $108^{\circ}43'–108^{\circ}57' E$) is a large macrophytic lake, the largest wetland at this latitude and very rare in desert and semi-desert regions (Figure 1). The annual mean precipitation and potential evaporation are 170 and 2300 mm, respectively. The lake has a mean surface elevation of 1019 m and a mean water depth of 1.4 m, with a surface area of 306 km^2 [33] and a mean annual temperature of $7.3 \text{ }^{\circ}\text{C}$. The ice-covered season lasts 100–130 day and the annual mean thickness of the ice is 0.63 m [34].

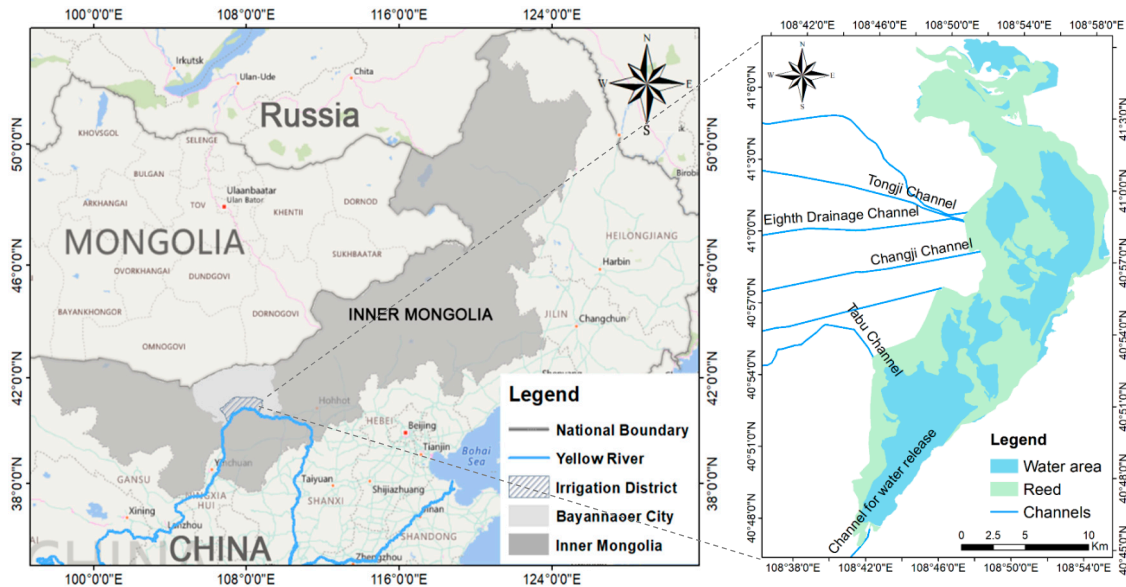


Figure 1. Location of Ulansuhai Lake.

2.2. Data Acquisition and Processing

The air temperature data of 1977–2014 and the daily mean temperature, humidity, cloudiness, precipitation, and evaporation data series of 2012–2013 (Figure 2) were acquired from meteorological station no. 53433 from the “China Meteorological Data” website [35]. These data, except evaporation, were used as the input variables for heat balance calculations; the daily mean evaporation series was used as a test parameter for the numerical calculations [36]. The entire heat balance calculation was implemented based on MATLAB R2012a, OriginPro 8.0, and Visual Fortran 6.

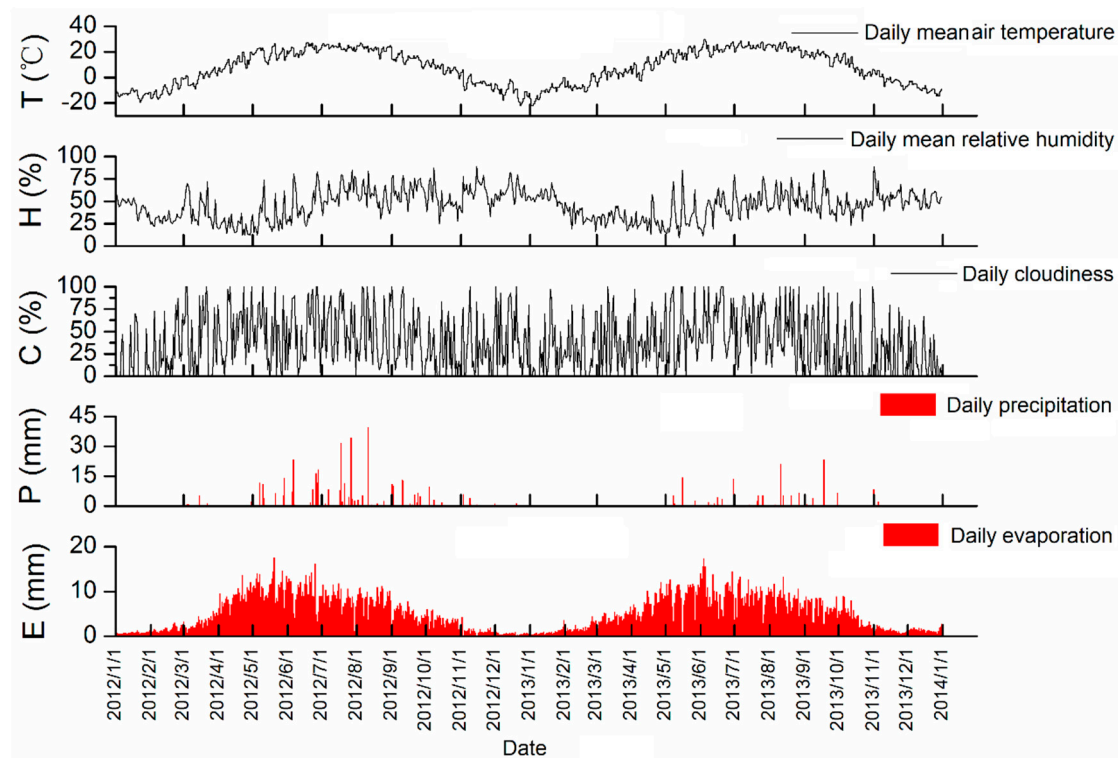


Figure 2. Daily mean temperature, humidity, cloudiness, precipitation, and evaporation in Ulansuhai Lake from 2012 to 2013.

2.3. Energy Budget Components of an Ice-Covered Lake

2.3.1. Intra-Annual Heat Balance Equation between the Lake Surface and the Atmosphere

The total heat content of the lake comprises latent heat and sensible heat. Taking the reference heat content U_0 to correspond to the liquid water phase at 0 °C, the heat content of the lake per unit area is expressed as $U = U_0 + E$, where

$$E = \int_{h_B}^{h_b} \rho_w c_w (T - T_f) dz + \int_{h_b}^{h_0} \rho_i [-(1 - \nu)L_f + c_i(T - T_f)] dz, \quad (1)$$

where h_0 , h_b , and h_B are the elevations of the upper surface of the ice, the bottom of the ice cover, and the bottom of the lake, respectively, ν is the volume fraction of liquid water occupied by the ice layer, ρ_w and ρ_i are the intrinsic densities of the liquid water and ice, respectively, c_w and c_i are the specific heats of liquid water and ice, respectively, L_f is the latent heat of freezing, T is the temperature, T_f is the freezing point, and z is the vertical coordinate. The snow layer is regarded as part of the ice layer.

Equation (1) is differentiated as follows:

$$\frac{dE}{dt} = Q_0 + \int_{h_B}^{h_0} \lambda Q_s dz - \kappa \left. \frac{\partial T}{\partial z} \right|_{z=h_B} + Q_A + Q_M, \quad (2)$$

where Q_0 is the surface heat balance, Q_s is the solar radiation, κ is the thermal conductivity, λ is the light attenuation coefficient, Q_A is the advective heat flux, and Q_M is the heat introduced by mass change. The direction of energy entering the lake is defined as a positive direction. The net surface heat flux is the dominant factor.

The intra-annual surface heat balance can be simplified as follows:

$$Q_n = Q_s + Q_L + Q_H + Q_e + Q_P, \quad (3)$$

where Q_n is the net solar and atmospheric heat flux to the lake surface, Q_s is the net solar radiation, Q_L is the net terrestrial radiation, Q_H and Q_e are the turbulent sensible and latent heat fluxes, and Q_P is the heat energy variation caused by precipitation.

2.3.2. Net Solar Radiation

Net solar radiation is the direct and diffuse radiation from the sun reaching the ground after being attenuated by the atmosphere. This quantity can be directly measured or estimated from astronomic and atmospheric data. According to Iqbal [37], the net solar radiation is influenced by solar elevation angle and atmospheric transparency, as:

$$Q_s = \cos Z T_{tr}(Z, e) F(N, Z) (r_0/r)^2 Q_{sc}, \quad (4)$$

where Z is the solar zenith angle—namely, the angle between the zenith direction and the sun, complement of the solar elevation angle, T_{tr} is the atmospheric clear sky transmittance [23], e is the atmospheric vapor pressure, F is a reduction due to cloudiness N ($0 \leq N \leq 1$) [38], r and r_0 are actual and mean Earth–Sun distances, respectively, and $Q_{sc} = 1367 \text{ W/m}^2$ is the solar constant (the value recommended by the World Meteorological Organization).

2.3.3. Net Terrestrial Radiation

Net terrestrial radiation is the difference between the thermal radiation received from the sky to the ground and the thermal emission from the lake water/ice surface. The surface emission is given by the gray body law:

$$Q_{L_0} = \varepsilon \sigma T_0^4, \quad (5)$$

where ε is the emissivity of water/ice/snow ($\varepsilon_{\text{water}} = 0.99$ and $\varepsilon_{\text{ice/snow}} = 0.97$), $\sigma = 5.67 \times 10^{-8} \text{ W/m}^2 \cdot \text{K}^4$ is the Stefan–Boltzmann constant, and T_0 is the absolute temperature of the surface.

Because it is difficult to obtain monitoring data for T_0 , this is estimated by the integral interpolation method described by Launiainen and Cheng [39]. The ice/water layer is discretized for a grid, and then the heat conduction through ice is gradually evaluated by iteration (Newton's iterative method) from the bottom (0°C) to the top (atmospheric temperature) of the ice cover. Finally, the temperature of the atmosphere–ice interface is taken as the ice surface temperature. The heat conduction equation of ice and the boundary conditions is expressed as follows:

$$\rho c(z, t) \frac{\partial T(z, t)}{\partial t} - \frac{\partial}{\partial z} \left(k(z, t) \frac{\partial T(z, t)}{\partial z} \right) = Q(z, t), \quad (6)$$

$$\begin{cases} T_f^k = T_f^t \\ T_{n_i}^k = T_b, \quad T_{n_s}^k = T_{in} \\ T_j^0 = T_i(z_j) \end{cases} \quad (7)$$

In Equation (7), k is the time step count for ∂t , and j is the layer count of ice. The boundary conditions reveal that the temperature in the last layer of ice is equal to the temperature of the upper surface of the ice. The temperature at the undersurface of the ice layer is the same as in the ice bottom. The temperature at the snow layer undersurface is equal to the temperature at the top surface of the ice cover, and the initial condition is set as the temperature at the undersurface of the ice cover equal to the ice–water interface.

Terrestrial radiation is a relatively complex quantity that is strongly affected by atmospheric conditions, such as water droplets, dust, and gas molecules, at different heights and temperatures. This radiation is estimated using Equation (8) [40]:

$$Q_{L_a} = \varepsilon_a \sigma T_a^4, \quad (8)$$

$$\varepsilon_a = \varepsilon_a(N, e) = (a + be^{1/2})(1 + cN^2), \quad (9)$$

where ε_a is the effective atmospheric emissivity, and a , b , and c are the constants 0.68, 0.036 m/bar^{1/2}, and 0.18, respectively.

2.3.4. Turbulent Heat Flux

The turbulent heat flux between the atmosphere and the lake surface consists of sensible heat flux and latent heat flux, calculated using the following equations:

$$Q_H = \rho_a c_p C_H (T_a - T_0) U_a, \quad (10)$$

$$Q_e = \rho_a L_E C_E (q_a - q_0) U_a, \quad (11)$$

where ρ_a and c_a are the density and specific heat capacity, respectively, of the atmosphere. $L_E = 2.5$ MJ/kg is the evaporation enthalpy, q_0 and q_a are the specific humidity at the lake surface and the air, respectively, at a height of 2 m near the lake surface [41], U_a is wind speed, C_H (Stanton constant) and C_E (Dalton constant) are heat exchange coefficients, which can be regarded as constants at standard atmospheric pressures, that is, 1.0×10^{-3} and 1.5×10^{-3} [42].

The calculation of turbulent heat flux coefficients is performed using the following equations [32]:

$$C_h = \kappa^2 \left(\ln \frac{z}{z_0} - \psi_M \frac{z}{L} \right)^{-1} \left(\ln \frac{z}{z_t} - \psi_h \frac{z}{L} \right)^{-1}, \quad (12)$$

$$C_e = \kappa^2 \left(\ln \frac{z}{z_0} - \psi_M \frac{z}{L} \right)^{-1} \left(\ln \frac{z}{z_q} - \psi_h \frac{z}{L} \right)^{-1}, \quad (13)$$

$$L = -u_3^* \bar{T} \rho_a c_p \left[g \kappa Q_h \left(1 + \frac{0.61 \bar{T} c_p Q_e}{Q_h L_e} \right) \right]^{-1}, \quad (14)$$

where $\kappa \approx 0.4$ is the von Kármán constant, ψ_M , ψ_h , and ψ_e are universal functions describing the influence of atmospheric surface stability on the gross heat conductivity, and $z/L = \zeta$ is a dimensionless height, and L is the Monin–Obukhov length (Equation (14)), in which the parameters are determined using the iterative method recommended by Launiainen and Vihma [43]. The wind speed data series U_a was obtained by interpolating the 8-h wind speed at 2-m height recorded at the monitoring station.

2.3.5. Precipitation

Precipitation affects the heat exchange at the upper surface of the ice cover via sensible heat and phase transitions. The sensible heat flux of precipitation can be neglected, but phase transitions may bring significant fluxes. This flux is expressed as:

$$Q_p = \rho [c(T_p - T_0) + L_f \chi_p] P, \quad (15)$$

where ρ and c are the density and specific heat capacity of the precipitation (liquid water or solid ice), respectively, $\chi_p = -1, 0$, or 1 represents the phase transitions of solid-to-liquid, no transition, or liquid-to-solid, respectively, $L_f = 335$ kJ/kg is the latent heat of freezing, T_p and T_0 are the temperatures of precipitation and lake surface, respectively, and P is precipitation, mm/day.

2.4. Simulation Test

The calculation results were verified using the radiation data from the Urad Front Banner meteorological station (National Meteorological Station no. 53336; 41°20'24'' N, 108°18'36'' E) in the study area. Because the maximum daily irradiance was relatively continuous, this quantity was compared with the calculated total solar radiation to test the calculation accuracy. The calculated value was equivalent to the daily mean total radiation, while the data from the meteorological station represented the daily maximum. The coefficient of determination R^2 was used as the statistical test parameter [44]. The calculation is shown in Equation (16):

$$R^2 = \sum_{i=1}^n (A_i - \bar{A})(S_i - \bar{S}) / \left[\sum_{i=1}^n (A_i - \bar{A})^2 \right]^{0.5} \left[\sum_{i=1}^n (S_i - \bar{S})^2 \right]^{0.5}, \quad (16)$$

where A_i is the testing sample, \bar{A} is the mean of the testing sample, S_i is the tested sample, and \bar{S} is the mean of the tested sample.

2.5. Selection of Typical Years

To ensure that the intra-annual heat balance at the lake surface possesses the climate characteristics of the study area, it is necessary to select typical years with the multiyear average climate characteristics. Here we determined the typical years based on multiyear air temperature data. The correlation coefficient of monthly cumulative average temperatures between 2012 and 2013 versus 2006–2014 reached 0.997 (Table 1). So, the meteorological data of 2012 and 2013 were used to estimate the intra-annual heat balance at the surface of Ulansuhai Lake.

Table 1. Correlation coefficient of monthly temperature from 2006 to 2014.

Year	2006–2014	2006	2007	2008	2009	2010	2011	2012	2013	2014
Monthly mean from 2006 to 2014	1									
2006	0.996	1								
2007	0.994	0.982	1							
2008	0.992	0.992	0.976	1						
2009	0.993	0.981	0.992	0.978	1					
2010	0.992	0.990	0.988	0.979	0.980	1				
2011	0.991	0.987	0.988	0.982	0.980	0.989	1			
2012	0.997	0.993	0.989	0.991	0.992	0.982	0.984	1		
2013	0.997	0.993	0.993	0.991	0.987	0.990	0.984	0.995	1	
2014	0.995	0.992	0.981	0.990	0.991	0.981	0.979	0.995	0.989	1

3. Results

3.1. Calculation of Thermodynamic Components

3.1.1. Net Solar Radiation Flux

Solar radiation is the main source of various thermal systems on Earth. It also plays a leading role in the heat balance system of lakes, especially in the northern lakes with seasonal ice cover. In the northern hemisphere spring, due to the enhancement of solar radiation, the water under the ice cover becomes warmer and the ice cover starts to ablate. During autumn and winter, because of the low level of solar radiation and air temperature, the lake loses heat via thermal radiation, conduction, and evaporation. The water temperature decreases continuously until it reaches a supercooled state, and then phase transition takes place, and the ice cover is formed with further heat loss (sketch of the surface energy balance in ice-covered lakes is shown in Figure 3).

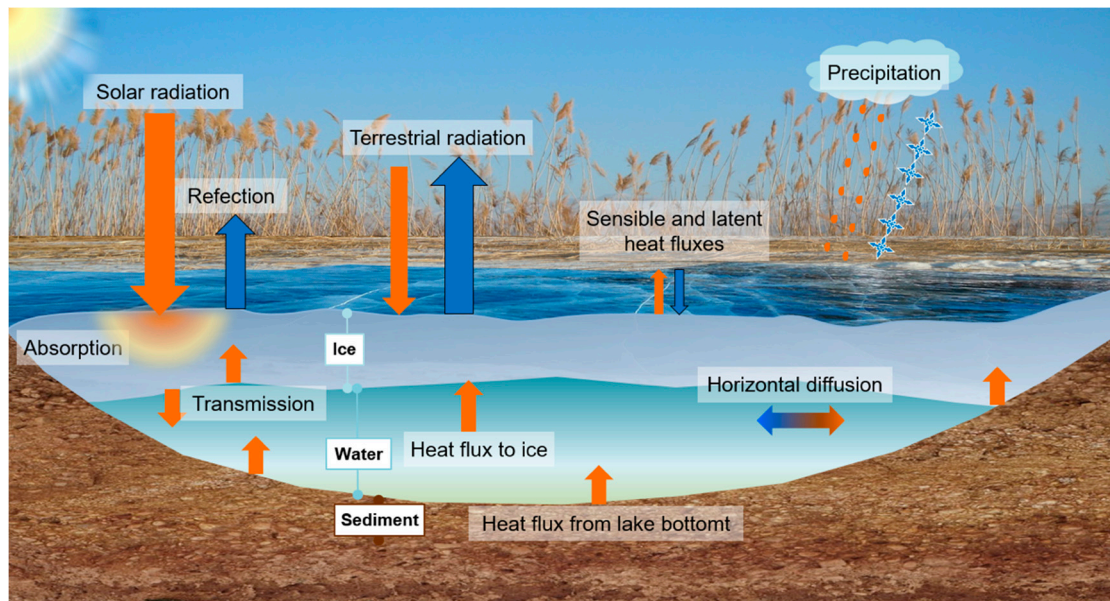


Figure 3. Sketch of the surface energy balance in ice-covered lakes. If the lake atmosphere is taken as the main body, upward arrows are positive, that is, there is energy from the lake to the atmosphere.

The net solar radiation showed similar features in 2012 and 2013. The mean flux was 210 W/m^2 and ranged from 0 to 828 W/m^2 in 2012, while in 2013 the mean flux was 179 W/m^2 and ranged from 0 and 758 W/m^2 . In 2012, the mean value was 78 W/m^2 in the ice-covered season and 228 W/m^2 in the open season. In the following year, the values in the ice-covered and open seasons were 68 W/m^2 and 229 W/m^2 , respectively. However, the growth rate of solar radiation was higher in the spring of 2013 than in the spring of 2012. In late February 2013, the net solar radiation had already increased to the level reached only in mid-March in 2012, more than 10 days difference. Consequently, the date of ice breakup was earlier in 2013 than in 2012. Solar radiation decreased more rapidly during the autumn of 2013 than in 2012. In early October 2013, the level had already reached the value recorded in mid-to-late October 2012.

The dynamic intra-annual variation of the total solar radiation in 2012 and 2013 compared with the daily maximum irradiances measured at the meteorological station. The R^2 values were 0.80 and 0.79 (by Equation (16)) for the total daily solar radiation flux of 2012 and 2013, respectively. This result indicated that the calculation accuracy generally met the requirements.

Solar radiation was relatively high in 2012. However, due to the long ice-covered season and thick ice cover, ice melting consumed a large portion of the radiation energy in 2012.

3.1.2. Net Terrestrial Radiation Flux

The distribution patterns of longwave radiation were generally similar in 2012 and 2013. Wintertime longwave radiation averaged -65.3 W/m^2 (-61.4 W/m^2) in 2012 (2013). The solar radiation arriving at the ground surface is not completely absorbed, as part of it is also reflected by the ground into the atmosphere. The reflectivity of surface objects to solar radiation depends on their surface properties and state. Generally, a light-colored object has a higher reflectivity than a dark one, and a smooth surface has a higher reflectivity than a rough surface. The reflectivity of a snow surface is considerably high at $\sim 60\%$, while the reflectivity of a still water surface is only $\sim 2\%$. In the northern hemisphere, the solar radiation is relatively intense during summer, while the reflectivity of the water surface is relatively low; therefore, most of the heat is used to warm the lake water. In early spring, the heat absorbed by the lake water melts the ice layer, which is responsible for warming the lake from $4 \text{ }^\circ\text{C}$ to the maximum water temperature. When the temperature rises, the characteristics of the high specific heat capacity of water begin to appear; part of the heat absorbed and stored by the

water in daytime is then lost at night in the form of radiation. Their longwave radiation state in the summertime is closer to the characteristics of terrestrial radiation compared with deep lakes and oceans. During winter, solar radiation energy is relatively low, but the snow-free ice cover also has high absorptivity. The absorbed energy is mainly used to prevent water from cooling in the early stage of freezing and is used for phase transition of ice in the initial stage of ice cover melting. Moreover, because the atmospheric radiation is much lower than terrestrial radiation in winter, the wintertime longwave radiation appears to be negative.

3.1.3. Turbulent Radiation Flux

The latent heat flux is represented mainly by heat loss due to evaporation from the water surface or sublimation from the ice surface. Occasionally, it may result in heat gain by condensation or deposition. Since the intensity of summertime solar radiation was greater in 2012 than in 2013, the latent heat loss in summer also followed the same trend (Figure 4a,b). In 2012, the intra-annual mean daily latent heat flux was -58.5 W/m^2 ($-213.8\sim 42.6 \text{ W/m}^2$). The daily mean latent heat flux was -38.6 W/m^2 during the ice-covered season, shifting to -68.6 W/m^2 during the open season. In 2013, the mean daily flux was -33.8 W/m^2 ($-196.1\sim 25.6 \text{ W/m}^2$). The daily mean was -44.4 W/m^2 during the ice-covered season and -12.3 W/m^2 during the open season. The latent heat released from the lake into the atmosphere was mainly from the evaporation of the water surface, in the ice season, the mean was the deposition of water vapor on a surface dominated by sublimation. Ice flowers on the surface were common scenery in winter.

Sensible heat flux is caused by the temperature difference between the atmosphere and the lake water surface. The air temperature is lower than the lake surface temperature during autumn and winter, which results in energy transfer from the lake to the atmosphere. Conversely, the air temperature is higher than the lake surface temperature in spring and summer, which results in energy transfer from the atmosphere into the lake. In 2012, the intra-annual daily mean sensible heat flux was -2.7 W/m^2 ($-33.4\sim 74.3 \text{ W/m}^2$). The monthly mean sensible heat flux was -1.5 W/m^2 during the ice-covered season, which changed to -20.0 W/m^2 during the open season. In 2013, the mean flux was -5.5 W/m^2 ($-34.6\sim 24.5 \text{ W/m}^2$). The monthly mean was 6.5 W/m^2 during the ice-covered season and -28 W/m^2 during the open season (Figure 4c,d).

To some extent, sensible and latent heat fluxes are synchronized in permanently ice-free lakes, such as Taihu Lake [25], because the phase transition only involves evaporation. However, the variation occurs earlier for sensible heat flux than for latent heat flux in seasonally ice-covered lakes, because the energy released by the phase transition of the ice cover has a delaying effect on the variation of sensible heat flux. For example, water does not freeze in the early stages before the temperature reaches the freezing point. It solidifies into ice and releases energy during the growth. The ice cover also damps the flow of heat from the lake to the atmosphere. Therefore, the ice cover provides a relatively stable temperature environment for aquatic life in winter. In spring, the solar radiation absorbed by the lake is mainly used for phase transition (solid-to-liquid). Even if the air temperature rises greatly in a short time, the minimum water temperature under the ice can remain above 0°C under the protection of the ice sheet. Hence the water temperature does not vary dramatically as long as the ice is present.

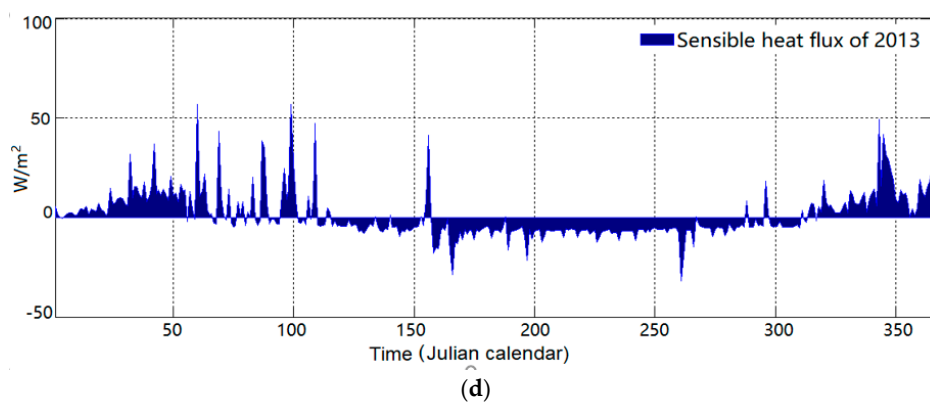
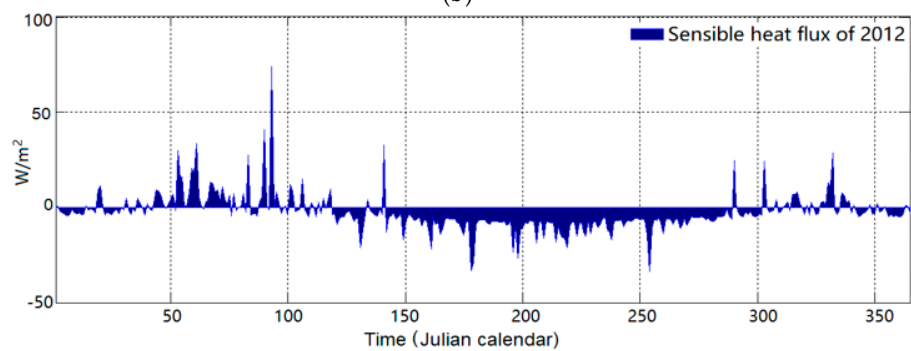
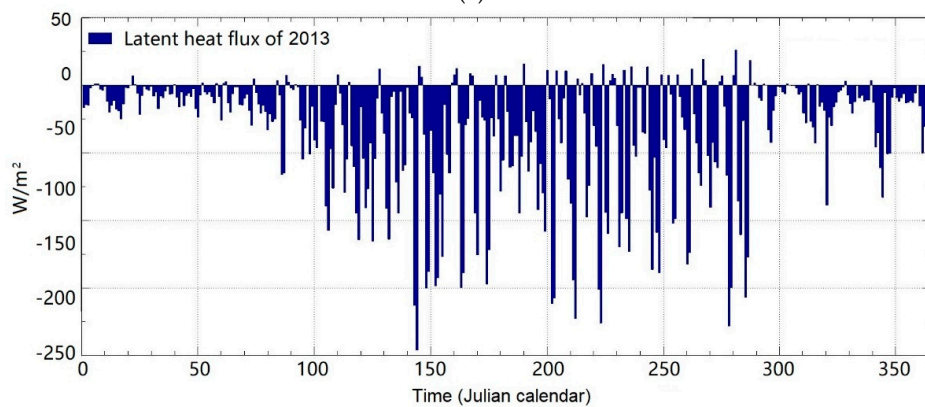
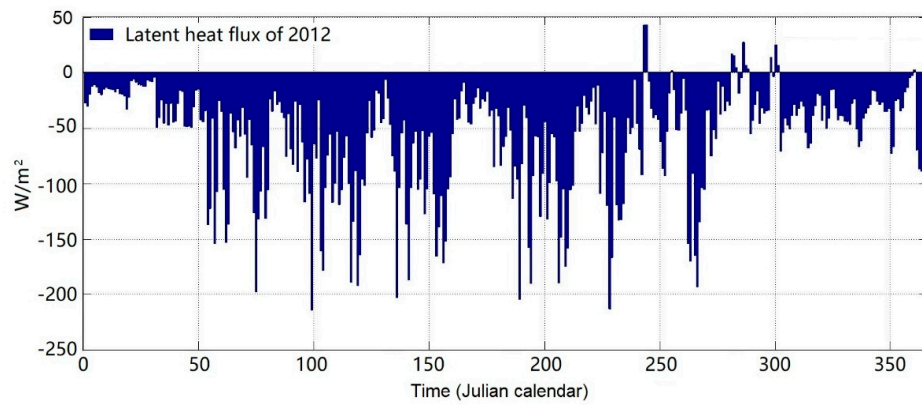


Figure 4. Turbulent radiation in 2012 and 2013. (a) Latent heat flux 2012, (b) latent heat flux 2013, (c) sensible heat flux 2012, (d) sensible heat flux 2013.

3.1.4. Precipitation Heat Flu

Precipitation heat fluxes are significant only in phase transitions. Positive values reveal that the precipitation undergoes a liquid–solid phase transition on the ice surface, and negative values indicate that snow falls onto the lake surface and absorbs energy to melt into water. Summer precipitation does not contribute much to lake heat content. Precipitation in Ulansuhai Lake is mainly concentrated in summer, while the winter is dry and windy with almost no snow accumulation on the lake surface. The winter precipitation heat flux averaged to 2 W/m^2 in 2012 and -1 W/m^2 in 2013 (Figure 5). A heat flux of less than 5 W/m^2 has a minor influence on the heat budget of the entire lake [45].

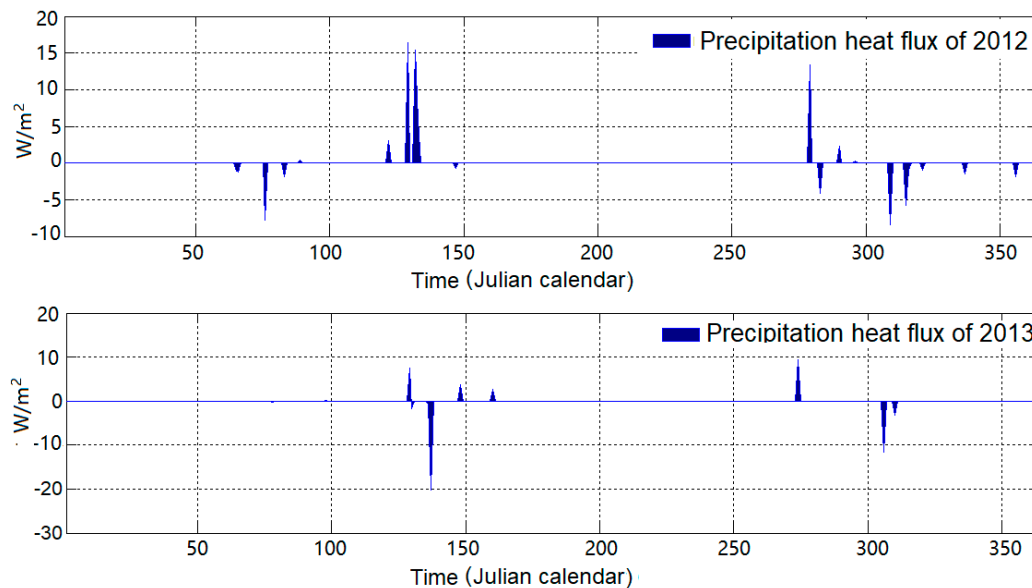


Figure 5. Precipitation heat flux variation in 2012 and 2013.

3.1.5. Net Heat Flux

Ulansuhai Lake gained heat on average 300 days per year in 2012 and 2013 (Figure 6). In 2012 (2013), the net heat flux averaged -33.8 W/m^2 (-38.5 W/m^2) during the ice-covered season, with a range between -74.8 and -1.3 W/m^2 (-125.2 and 7.1 W/m^2). The net heat flux averaged 62.4 W/m^2 (19.1 W/m^2) during the open season, with a range from -95.8 to 272.1 W/m^2 (from -125.2 to 122.1 W/m^2).

During the open season, the net heat flux was positive and the exchange was intense. This is because Ulansuhai Lake is shallow and has high solar radiation flux in summer. The lake water absorbs energy that raises the water temperature and conducts heat downward to the sediment. Since the small volume of a shallow lake has a limited heat storage capacity, the sediment becomes another main area for the storage of lacustrine heat. If the lake water has high transparency and the sediment deposits are rich in organic matter and dark in color, the sediment absorbs solar energy directly and the water temperature can rise faster. Moreover, due to the frequent windy weather and high water vapor transfer intensity over the lake, the evaporation of the shallow lake is high.

During the ice-covered season, the lake water temperature is higher than the atmospheric temperature. Latent heat is released from the formation of ice, and the amount of ice remains limited since this heat needs to be conducted through the ice. Therefore, the ice-covered season is in a heat-loss state. When the ice cover has formed, it blocks the direct contact between the water and the atmosphere that plays a key role in suppressing the heat loss. Under these conditions, the heat stored at the lake bottom is continuously delivered to lake water. In addition to sunlight, this is the only pathway to obtain heat in the water under the ice. The ice cover ensures that the lake water can provide a suitable environmental temperature for maintaining aquatic life, even if the external air temperature is around $-20 \text{ }^\circ\text{C}$.

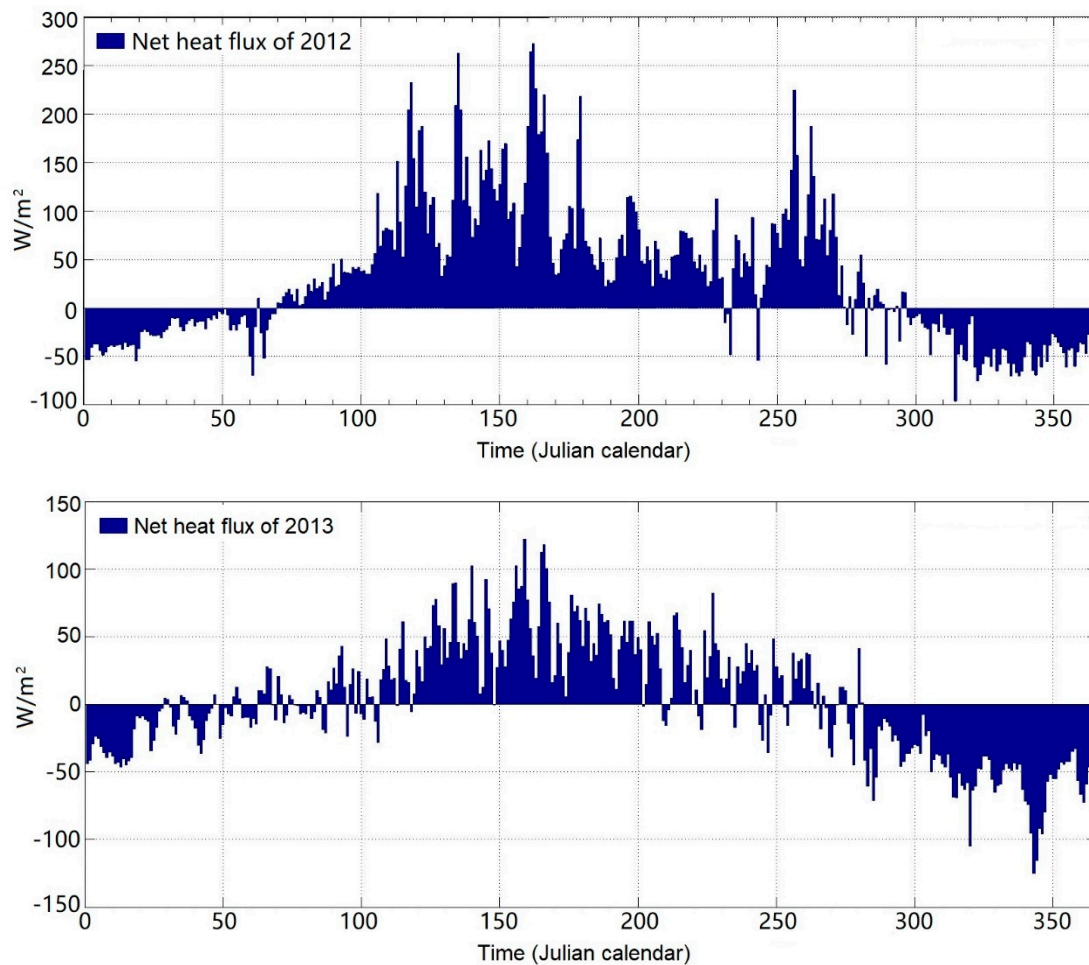


Figure 6. Net heat flux in 2012 and 2013.

4. Discussion

4.1. Influence of Wind on Seasonal Lakes

The wind is an important driver of hydrodynamic processes in shallow lakes and it plays a decisive role in the transfer, transport, and diffusion of material and energy in lakes [23,28]. The wind has two main effects on the ice cover of shallow lakes in the ice season. Firstly, in the early stage of freezing, the ice cover is fragile and can be easily broken by the force of the wind. For example, in Ulansuhai and Hulun lakes in Inner Mongolia, the weather is often windy in the winter. When the initial ice cover (thickness of 3–5 cm) breaks up, the crushed ice is driven toward the shore by winds until the kinetic energy flux is consumed by friction, and the ice piles up and rides on the shore. With the decreasing air temperature, the broken ice is consolidated to form a new ice cover on the leeward side with an uneven surface. In the upwind direction, the new ice cover is regenerated into the open lake water with a smooth surface [34]. The smooth ice often does not accumulate snow or form a snow cover when windy weather is frequent in winter, but snow-covered patches exist in the rough ice. Because of the high albedo of the snow surface [13,42], light cannot easily pass through snow-covered ice to reach the deeper water. In the winter, this phenomenon, to some extent, also inhibits photosynthetic capacity and has a consequent influence on the aquatic ecosystem.

Ulansuhai Lake is a representative lake in the Inner Mongolian Plateau of northern China, which is mainly controlled by the temperate, arid climate [46]. Northwesterly winds are prevalent in the lake throughout the year (Figure 7), with a calm frequency of 8.5%. The frequency of northwesterly winds in the ice season is higher than in the open season, with a calm frequency of 20.2%. This is because

of the influence of the temperate monsoon climate from the southeast in summer, which has a calm frequency of 16.5%. The wind speeds appeared to be higher in the spring and lower in the autumn in both 2012 and 2013. The mean wind speed in 2012 was 1.5 m/s, with a maximum of 5.9 m/s, and in 2013 these were, respectively, 1.6 m/s and 7.8 m/s (Figure 8). The lake surface experienced a windy state year-round that is also an important factor leading to intensive surface water evaporation.

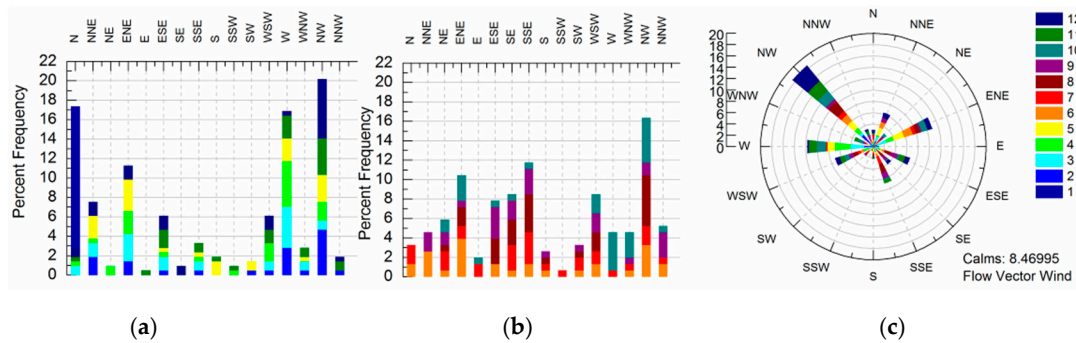


Figure 7. Wind direction frequency of Ulansuhai Lake from 2012 to 2013. (a) Ice-covered season, (b) open season, (c) the whole year.

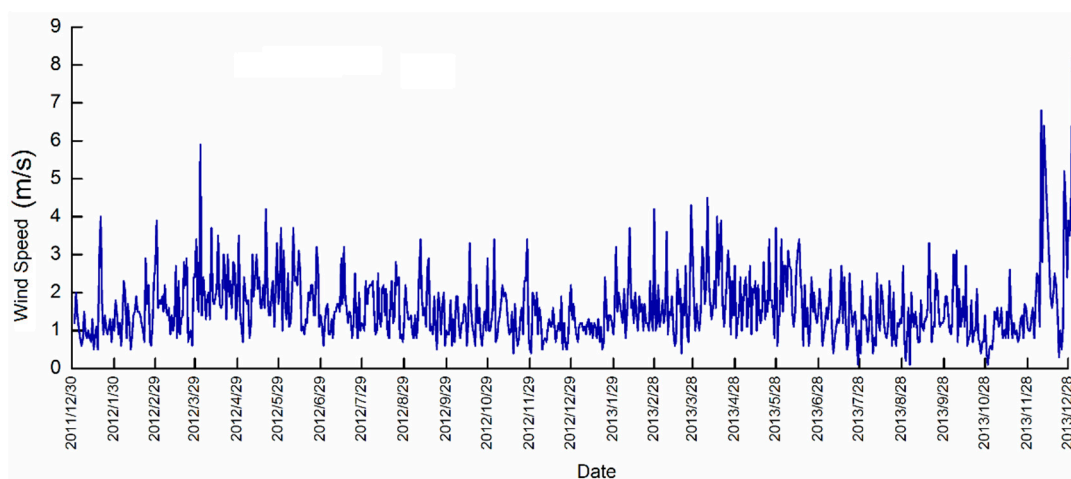


Figure 8. Daily wind speed of Ulansuhai Lake in 2012 and 2013 (taken from 2-m height).

During the open season, the wind and wave effects are conducive to gas exchange between the lake water and the atmosphere [8,20,25]. However, in a lake with an endogenous pollution problem, stirring the lake water increases the intensity of nutrients and pollutants released from sediments. In the early stage of freezing, windy weather leads to the smooth ice formation in the northwestern region of the lake. Meanwhile, rough ice is formed by the aggregation and freezing in the southeastern region. These formation patterns affect the distribution of surface snow and even influence aquatic ecosystems under the ice [36]. When simulating the initial freezing and melting, the heat flux in shallow lakes is considerably disturbed by the wind force during the early spring and late autumn. In early freezing and late melting periods, the mechanical forcing of wind may break the ice cover and forced displacements. Then the surface and, further, the heat fluxes are strongly modified [32], and thermal and mechanical forcing consists of a coupled system.

4.2. Mechanism of Intra-Annual Heat Exchange Process in an Ice-Covered Lake

A correlation analysis was performed on the monthly temperature data in 2004–2014 to select the years representative of typical temperature variations over the past 10 years. The climate in northern China entered a new 30-year cold cycle starting around the year 2000 [47,48]. From the period 1977–2014 to 2006–2014 (Figure 9), the mean monthly air temperature dropped by 1.7–2.2 °C.

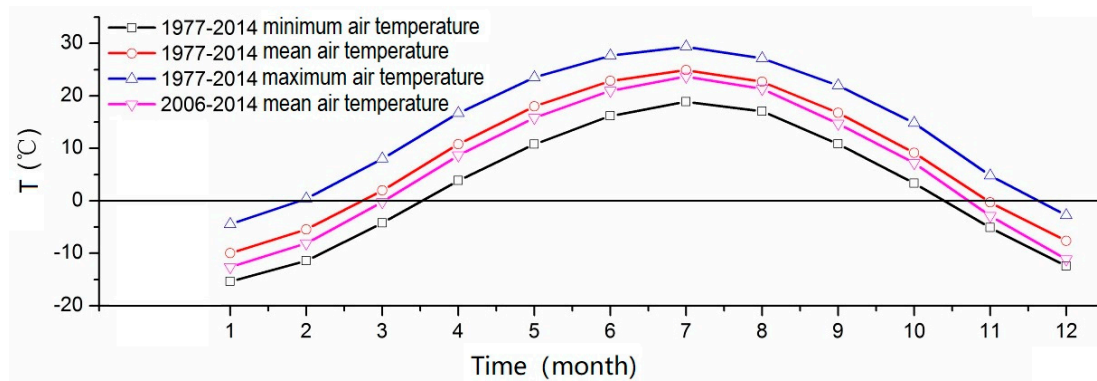


Figure 9. Monthly temperature comparison for the years 1977–2014 and 2006–2014.

A sketch of surface energy balance in ice-covered lakes is shown in Figure 3. When the ice has few impurities, the solar radiation that passes through the ice layer to reach the underwater layer not only plays a crucial role in the ice ablation but also has a strong influence on lake photosynthesis in winter. When the precipitation takes the form of a solid phase (e.g., snow and hail), it decreases the energy of the lake; when it is in a liquid phase ($>0\text{ }^{\circ}\text{C}$), the energy of the lake system increases [13,32]. At the ice–water interface, thermal energy transmits from the water layer to the ice, the heat flux from water takes 5 W/m^2 as a reference value [33], while the release and absorption of latent heat are determined by the growth and ablation of the ice cover [29,36].

5. Conclusions

(1) Comparing the monthly temperatures in 1977–2014 and 2006–2014, we found that the mean temperature dropped by $1.7\text{--}2.2\text{ }^{\circ}\text{C}$ compared with the past 50 years. We selected 2012 and 2013 as typical for the simulation. The simulated net solar radiation flux showed a similar evolution with the maximum daily irradiance, $R^2 \approx 0.8$. The model can therefore be used to describe the intra-annual heat flux variation in the lake area.

(2) The solar radiation was relatively high in the shallow lake in northern China, with a mean net solar radiation flux of 197.5 W/m^2 in 2012–2013. The intra-annual heat budget substantially differed between the ice-covered and open seasons. The net solar radiation averaged 73 W/m^2 during the ice season, while it changed to 228.5 W/m^2 during the open season. Precipitation had little influence on the heat budget of the entire lake.

(3) Northwesterly winds were prevalent in Ulansuhai Lake throughout the year. The calm frequency of northwesterly winds was 20.2% during the ice-covered season. The lake area was influenced by the temperate monsoon climate from the southeast direction during summer, with a calm frequency of 16.5%. The wind speed appeared to be higher in spring and lower in autumn for both 2012 and 2013. Winds had an influence on the climate of the lake for both the ice-covered and open seasons during the simulations. Summer was an important factor for intensive evaporation, while winter was a strong driver of ice cover formation.

In summary, the heat content of lakes mainly comes from the heat energy reserve in summer. Following ice-cover formation in winter, there is no substantial water temperature variation in shallow lakes. Heat exchange between the ice surface and the atmosphere is the major factor for ice growth and ablation. Understanding heat exchange above the ice cover can provide a clear physical background for the simulation of ice thickness in lakes.

Author Contributions: F.Y. contributed to Writing-original draft. W.F. contributed to Writing-editing. L.M. contributed to heat transfer estimation methods and participation in data analysis. Y.Y. contributed to Data curation. I.M. contributed to code programming. R.C., Y.B. and C.L. contributed to Investigation. H.L. helped perform the analysis with constructive discussions. All authors have read and agreed to the published version of the manuscript.

Funding: This research was jointly supported by the National Natural Science Foundation of China (grant numbers YFC0409205, 51779117, 41907338, and 41703115), and Postdoctoral Science Foundation of China (2019M660753), Welfare Scientific Subject of CRAES (JY-2011ZX07212-007-001), and Youth Top Talent Support Program of Beihang University (YWF-20-BJ-J-907).

Conflicts of Interest: The authors declare no conflict of interest.

References

- Adrian, R.; Reilly, C.M.O.; Zagarese, H.; Baines, S.B.; Hessen, D.O.; Keller, W.; Livingstone, D.M.; Sommaruga, R.; Straile, D.; Van Donk, E.; et al. Lakes as sentinels of climate change. *Limnol. Oceanogr.* **2009**, *54*, 2283–2297. [[CrossRef](#)] [[PubMed](#)]
- Battin, T.J.; Luysaert, S.; Kaplan, L.A.; Aufdenkampe, A.K.; Richter, A.; Tranvik, L.J. The boundless carbon cycle. *Nat. Geosci.* **2009**, *2*, 598–600. [[CrossRef](#)]
- Feng, J.; Liu, H.; Wang, L.; Du, Q.; Shi, L. Seasonal and inter-annual variation of surface roughness length and bulk transfer coefficients in a semiarid area. *Sci. China Earth Sci.* **2011**, *55*, 254–261. [[CrossRef](#)]
- Guo, W.D.; Wang, X.; Sun, J.; Ding, A.; Zou, J. Comparison of land–atmosphere interaction at different surface types in the mid to lower reaches of the Yangtze River valley. *Atmos. Chem. Phys. Discuss.* **2016**, *16*, 9875–9890. [[CrossRef](#)]
- Liu, Y.; Guo, W.; Song, Y. Estimation of key surface parameters in semi-arid region and their impacts on improvement of surface fluxes simulation. *Sci. China Earth Sci.* **2015**, *59*, 307–319. [[CrossRef](#)]
- Butcher, J.; Nover, D.; Johnson, T.E.; Clark, C.M. Sensitivity of lake thermal and mixing dynamics to climate change. *Clim. Chang.* **2015**, *129*, 295–305. [[CrossRef](#)]
- Kraemer, B.M.; Hook, S.; Huttula, T.; Kotilainen, P.; O’Reilly, C.M.; Peltonen, A.; Plisnier, P.-D.; Sarvala, J.; Tamatamah, R.; Vadeboncoeur, Y.; et al. Century-long warming trends in the upper water column of lake Tanganyika. *PLoS ONE* **2015**, *10*, e0132490. [[CrossRef](#)]
- Piccolroaz, S. Prediction of lake surface temperature using the air2water model: Guidelines, challenges, and future perspectives. *Adv. Oceanogr. Limnol.* **2016**, *7*, 36–50. [[CrossRef](#)]
- Piccolroaz, S.; Toffolon, M.; Majone, B. The role of stratification on lakes’ thermal response: The case of Lake Superior. *Water Resour. Res.* **2015**, *51*, 7878–7894. [[CrossRef](#)]
- Sahoo, G.B.; Forrest, A.L.; Schladow, S.G.; Reuter, J.E.; Coats, R.; Dettinger, M. Climate change impacts on lake thermal dynamics and ecosystem vulnerabilities. *Limnol. Oceanogr.* **2015**, *61*, 496–507. [[CrossRef](#)]
- Wood, T.M.; Wherry, S.A.; Piccolroaz, S.; Girdner, S.F. *Simulation of Deep Ventilation in Crater Lake, Oregon, 1951–2099*; Scientific Investigations Report 2016-5046; U.S. Geological Survey: Reston, VA, USA, 2016.
- Venäläinen, A.; Frech, M.; Heikinheimo, M.; Grelle, A. Comparison of latent and sensible heat fluxes over boreal lakes with concurrent fluxes over a forest: Implications for regional averaging. *Agric. For. Meteorol.* **1999**, *98*, 535–546. [[CrossRef](#)]
- Leppäranta, M.; Lindgren, E.; Shirasawa, K. The heat budget of Lake Kilpisjärvi in the Arctic tundra. *Hydrol. Res.* **2017**, *48*, 969–980. [[CrossRef](#)]
- Crosman, E.T.; Horel, J.D. Sea and lake breezes: A review of numerical studies. *Bound. Layer Meteorol.* **2010**, *137*, 1–29. [[CrossRef](#)]
- Steyn, D.G. Scaling the vertical structure of sea breezes revisited. *Bound. Layer Meteorol.* **2003**, *107*, 177–188. [[CrossRef](#)]
- Feng, W.; Wu, F.; He, Z.; Song, F.; Zhu, Y.; Giesy, J.P.; Wang, Y.; Qin, N.; Zhang, C.; Chen, H.; et al. Simulated bioavailability of phosphorus from aquatic macrophytes and phytoplankton by aqueous suspension and incubation with alkaline phosphatase. *Sci. Total. Environ.* **2018**, *616–617*, 1431–1439. [[CrossRef](#)] [[PubMed](#)]
- Flagg, D.; Brook, J.; Sills, D.; Makar, P.; Taylor, P.; Harris, G.; McLaren, R.; King, P. Lake breezes in southern Ontario: Observations, models and impacts on air quality. In *Air Pollution Modeling and Its Application XIX*; NATO Science for Peace and Security Series Series C: Environmental Security; Springer: Dordrecht, The Netherlands, 2008; pp. 679–680. [[CrossRef](#)]
- Sills, D.M.L.; Brook, J.R.; Levy, I.; Makar, P.A.; Zhang, J.; Taylor, P.A. Lake breezes in the southern Great Lakes region and their influence during BAQS-Met 2007. *Atmos. Chem. Phys. Discuss.* **2011**, *11*, 7955–7973. [[CrossRef](#)]

19. Feng, J.W.; Liu, H.Z.; Sun, J.H.; Wang, L. The surface energy budget and interannual variation of the annual total evaporation over a highland lake in Southwest China. *Theor. Appl. Clim.* **2016**, *126*, 303–312. [CrossRef]
20. Ning, L.; Zhan, C.; Luo, Y.; Wang, Y.; Liu, L. A review of fully coupled atmosphere-hydrology simulations. *J. Geogr. Sci.* **2019**, *29*, 465–479. [CrossRef]
21. Decker, M.; Zeng, X. Impact of modified Richards equation on global soil moisture simulation in the Community Land Model (CLM3.5). *J. Adv. Model. Earth Syst.* **2009**, *1*, 1–22. [CrossRef]
22. Subin, Z.M.; Mironov, D.; Riley, W.J. An improved lake model for climate simulations: Model structure, evaluation, and sensitivity analyses in CESM1. *J. Adv. Model. Earth Syst.* **2012**, *4*, 1–27. [CrossRef]
23. Sun, S.; Yan, J.; Xia, N.; Li, Q. The model study of water mass and energy exchange between the inland water body and atmosphere. *Sci. China Ser. G Phys. Mech. Astron.* **2008**, *51*, 1010–1021. [CrossRef]
24. Cheng, X.; Wang, Y.; Cheng, H.U.; Wang, W.; Zhang, M.; Xiao, Q.; Liu, S.; Xuhui, L. The lake-air exchange simulation of a lake model over eastern Taihu Lake based on the turbulent kinetic energy closure thermodynamic process. *Acta Meteorol. Sin.* **2016**, *74*, 633–645. [CrossRef]
25. Deng, B.; Liu, S.; Xiao, W.; Wang, W.; Jin, J.; Lee, X. Evaluation of the clm4 lake model at a large and shallow freshwater lake. *J. Hydrometeorol.* **2013**, *14*, 636–649. [CrossRef]
26. Dai, Y.; Qiu, Y.; Piao, M.; Wang, Y. Analyzing the impact of buildings on surrounding temperature observational environment. In Proceedings of the International Conference on Remote Sensing, Environment and Transportation Engineering, Nanjing, China, 26–28 July 2013.
27. Hongpin, G.U.J.M.M. Evaluation on simulation of coupled WRF-lake model to lake surface temperature in Taihu Lake. *Meteorol. Mon.* **2014**, *40*, 166–173. [CrossRef]
28. Kirilin, G.; Leppäranta, M.; Terzhevik, A.; Granin, N.; Bernhardt, J.; Engelhardt, C.; Efremova, T.; Golosov, S.; Palshin, N.; Sherstyankin, P.; et al. Physics of seasonally ice-covered lakes: A review. *Aquat. Sci.* **2012**, *74*, 659–682. [CrossRef]
29. Sugiyama, N.; Kravtsov, S.; Roebber, P. Multiple climate regimes in an idealized lake-ice-atmosphere model. *Clim. Dyn.* **2017**, *50*, 655–676. [CrossRef]
30. Van Cleave, K.; Lenters, J.D.; Wang, J.; Verhamme, E.M. A regime shift in Lake Superior ice cover, evaporation, and water temperature following the warm El Niño winter of 1997–1998. *Limnol. Oceanogr.* **2014**, *59*, 1889–1898. [CrossRef]
31. Ferris, J.M.; Burton, H.R. The annual cycle of heat content and mechanical stability of hypersaline Deep Lake, Vestfold Hills, Antarctica. *Hydrobiologia* **1988**, *165*, 115–128. [CrossRef]
32. Merkouridi, I.; Leppäranta, M.; Shirasawa, K. Seasonal and annual heat budgets offshore the Hanko Peninsula, Gulf of Finland. *Boreal Environ. Res.* **2013**, *18*, 89–108.
33. Song, S.; Li, C.; Shi, X.; Zhao, S.; Tian, W.; Li, Z.; Bai, Y.; Cao, X.; Wang, Q.; Huotari, J.; et al. Under-ice metabolism in a shallow lake in a cold and arid climate. *Freshw. Biol.* **2019**, *64*, 1710–1720. [CrossRef]
34. Fang, Y.; Changyou, L.; Leppäranta, M.; Xiaonghong, S.; Shengnan, Z.; Chengfu, Z. Notable increases in nutrient concentrations in a shallow lake during seasonal ice growth. *Water Sci. Technol.* **2016**, *74*, 2773–2783. [CrossRef] [PubMed]
35. China Meteorological Data. Available online: <http://data.cma.cn/data> (accessed on 20 August 2020).
36. Huang, W.; Zhang, J.; Leppäranta, M.; Li, Z.; Cheng, B.; Lin, Z. Thermal structure and water-ice heat transfer in a shallow ice-covered thermokarst lake in central Qinghai-Tibet Plateau. *J. Hydrol.* **2019**, *578*, 124122. [CrossRef]
37. Iqbal, M. *An Introduction to Solar Radiation*; Academic Press: New York, NY, USA, 1983; pp. 387–390.
38. Lumb, F.E. The influence of cloud on hourly amounts of total solar radiation at the sea surface. *Q. J. R. Meteorol. Soc.* **1964**, *90*, 43–56. [CrossRef]
39. Launiainen, J.; Cheng, B. Modelling of ice thermodynamics in natural water bodies. *Cold Reg. Sci. Technol.* **1998**, *27*, 153–178. [CrossRef]
40. Omstedt, A. Modelling the Baltic Sea as thirteen sub-basins with vertical resolution. *Tellus A Dyn. Meteorol. Oceanogr.* **1990**, *42*, 286–301. [CrossRef]
41. Kirilin, G.; Aslamov, I.; Leppäranta, M.; Lindgren, E. Turbulent mixing and heat fluxes under lake ice: The role of seiche oscillations. *Hydrol. Earth Syst. Sci.* **2018**, *22*, 6493–6504. [CrossRef]
42. Andreas, E.L. A theory for the scalar roughness and the scalar transfer coefficients over snow and sea ice. *Bound. Layer Meteorol.* **1987**, *38*, 159–184. [CrossRef]

43. Launiainen, J.; Vihma, T. Derivation of turbulent surface fluxes—An iterative flux-profile method allowing arbitrary observing heights. *Environ. Softw.* **1990**, *5*, 113–124. [[CrossRef](#)]
44. Moriasi, D.N.; Arnold, J.G.; Van Liew, M.W.; Bingner, R.L.; Harmel, R.D.; Veith, T.L. Model evaluation guidelines for systematic quantification of accuracy in watershed simulations. *Trans. ASABE* **2007**, *50*, 885–900. [[CrossRef](#)]
45. Leppäranta, M. A review of analytical models of sea-ice growth. *Atmos. Ocean.* **1993**, *31*, 123–138. [[CrossRef](#)]
46. Zhao, N.; Liang, S.; Ding, Y. Underlying low-order dynamics of nonlinear interaction among northern hemisphere teleconnection patterns and its association with the AO/NAM. *J. Clim.* **2014**, *27*, 1315–1335. [[CrossRef](#)]
47. Ding, Y.; Liu, Y.; Liang, S.; Ma, X.; Zhang, Y.; Si, D.; Liang, P.; Song, Y.; Zhang, J. Interdecadal variability of the East Asian winter monsoon and its possible links to global climate change. *J. Meteorol. Res.* **2014**, *28*, 693–713. [[CrossRef](#)]
48. Jia, X.; Lin, H.; Ge, J. The interdecadal change of ENSO impact on wintertime East Asian climate. *J. Geophys. Res. Atmos.* **2015**, *120*, 918–935. [[CrossRef](#)]



© 2020 by the authors. Licensee MDPI, Basel, Switzerland. This article is an open access article distributed under the terms and conditions of the Creative Commons Attribution (CC BY) license (<http://creativecommons.org/licenses/by/4.0/>).